A Comparison of Long Coastal Trapped Wave Theory with Observations off Peru[1]

K. H. BRINK

Woods Hole Oceanographic Institution, Woods Hole, MA 02543

(Manuscript received 1 December 1981, in final form 22 April 1982)

ABSTRACT

The agreement between coastal trapped wave theory and observation is studied for the case of observations made off Peru during the 1977 CUEA JOINT-II experiment. Wave properties are calculated using a numerical model with realistic, horizontally uniform stratification and realistic bottom topography. These properties are then explored as a function of the ratio of the first internal Rossby radius of deformation to the shelf-slope width. The agreement of observed and calculated first-mode, free wave phase speeds (230 cm s^{-1}) is excellent, while modal structures agree more poorly. A forced wave calculation, using observed winds and currents as input, is used to hindcast alongshore currents and sea level in the frequency band where Smith (1978) observed free coastal trapped waves during 1977. The model suggests that most of the observed sea level and alongshore velocity fluctuations in the 5–10 day period band are due to free waves originating equatorward of 5°S, while winds between 5°S and 15°S contribute little to the observed variance. Finally, free coastal trapped wave calculations are briefly compared with CUEA observations from off Northwest Africa and Oregon. Generally, the wave calculations appear to be a useful tool in interpretation of the field observations.

1. Introduction

Perhaps the most striking characteristic of the subinertial fluctuations in sea level and alongshore velocity observed during the 1977 CUEA JOINT-II experiment off the Peru coast is the importance of apparently free poleward-propagating, long coastal trapped waves. Smith (1978), Brink *et al.* (1980; hereafter BHS) and Romea and Smith (1982; hereafter RS) discussed the observed properties of these waves and RS detected them from 17.5°S all the way to 0°27′S. Although there is some evidence that the waves are fundamentally similar to baroclinic Kelvin waves, this has not been entirely substantiated. Also, the influence or lack of influence of the alongshore winds—the obvious driving mechanism for this sort of wave—has not been rationalized. These, and other considerations, boil down to the question: how well can the Peru coastal trapped wave observations be explained in light of existing theory?

The most useful body of theory for direct comparison with coastal trapped wave observations involves models with continuous stratification and realistic bottom topography (Wang and Mooers, 1976; Clarke, 1977; Huthnance, 1978; Brink, 1982). These studies, taken together, present the properties of the generalized (or hybrid) coastal trapped waves and of their parametric relation to the internal Kelvin and barotropic continental shelf wave limits. This type of wave model is used in the following to address specific questions on the applicability of the existing theory. For example, how good is the quantitative agreement between the free wave models and observations? Can the models accurately predict current and sea level fluctuations? What are the limitations on the applicability of coastal trapped wave theory to coastal regions other than that of Peru?

The following discussion will be centered on the main JOINT-II mooring line (the C-line) located on the continental shelf and slope near 15°S during March–May 1977. An overall description of this data set can be found in BHS. This central line consisted of seven current meter moorings with a total of 32 fully functional instruments. Also, five other current meter moorings were located at other latitudes, and various wind and sea level records were available. A more complete account of the alongshore array may be found in RS. Much of this information is utilized in the following, and the distribution of instrumentation largely determined the geographical emphasis of this study. Unless otherwise stated, all time series have been low-pass filtered with a half-power point of 1.96 days. The right-handed coordinate system used is consistent with RS: the x coordinate increases in the local onshore direction and y is positive in the equatorward direction. The reader should bear in mind that $f < 0$ for all calculations presented here.

2. Wave dynamics

a. The mathematical model

We wish to compute the free coastal trapped wave frequencies (eigenvalues) and the offshore-vertical

[1] W.H.O.I. Contribution No. 5055.

0022-3670/82/080897-17$08.25

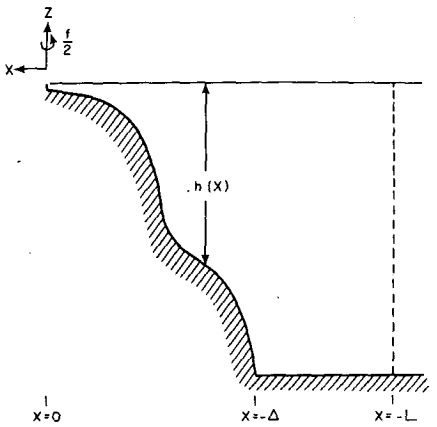

FIG. 1. Schematic of model geometry.

modal structures (eigenfunctions) for an alongshore wavenumber l, given the stratification and shelf-slope bottom topography of a region. We will consider a linear, inviscid problem with constant rotation where the stratification is horizontally uniform and the bottom topography does not vary in the alongshore direction. This problem has also been addressed by Wang and Mooers (1976) and by Huthnance (1978). With the above assumptions, the equations of motion are

$$u_t - fv = -\frac{1}{\rho_0} p_x , \tag{2.1a}$$

$$v_t + fu = -\frac{1}{\rho_0} p_y , \tag{2.1b}$$

$$0 = -p_z - g\rho, \tag{2.1c}$$

$$0 = u_x + v_y + w_z , \tag{2.1d}$$

$$0 = \rho_t + w\rho_{0z} , \tag{2.1e}$$

where u, v and w are the onshore, alongshore and vertical velocity components, $\rho(x, y, z, t)$ is the density perturbation from a rest state $\rho_0(z)$, p is the pressure perturbation, f the Coriolis parameter, g the acceleration due to gravity, and subscripts (x, y, z, t) denote partial differentiation. The geometry is shown in Fig. 1. System (2.1) reduces to

$$0 = p_{xxt} + p_{yyt} + \left(f^2 + \frac{\partial^2}{\partial t^2}\right)\left(\frac{p_z}{N^2}\right)_{zt} , \tag{2.2a}$$

where the Brunt-Väisälä frequency is defined as

$$N^2(z) \equiv -g\rho_0^{-1}\rho_{0z} .$$

The appropriate boundary conditions are

$$p_{zt} + N^2 g^{-1} p_t = 0 \quad \text{at} \quad z = 0, \tag{2.2b}$$

$$\left(f^2 + \frac{\partial^2}{\partial t^2}\right)p_{zt} + N^2 h_x (p_{xt} + fp_y) = 0 \quad \text{at} \quad z = -h(x), \tag{2.2c}$$

$$p_{xt} + fp_y = 0 \quad \text{at} \quad x = 0, \tag{2.2d}$$

$$p \to 0 \quad \text{as} \quad x \to -\infty, \tag{2.2e}$$

where $h(x)$ is the local depth of the ocean. The first condition represents a free surface, while the second and third follow from no normal flow at the bottom and at a coastal wall, respectively. The final condition expresses coastal trapping.

In order to find the free coastal trapped waves, we assume

$$p = \hat{p}(x, z) \exp[i(\omega t + ly)], \tag{2.3}$$

so that the system (3.2) becomes a two-dimensional eigenvalue problem. In general, numerical techniques must be employed to proceed further. Since only a limited spatial domain can be covered by a finite difference scheme, condition (2.2e), expressing coastal trapping, must be modified. A simple study of alternate offshore boundary conditions (see Appendix A) shows that the outer boundary condition

$$u_x = 0 \quad \text{at} \quad x = -L \tag{2.4}$$

is well behaved and computationally simple. The problem is solved on a 17×25 vertically stretched grid, such that there are always 17 grid points in the vertical, regardless of the total depth. Thus, resolution improves in shallower water. Typical horizontal resolution is about 8 km, but varies somewhat so that a sufficiently large amount of the deep, flat-bottomed ocean can be included in light of considerations in Appendix A. The problem for a given l is solved by resonance iteration for ω, solving the matrix equation by a direct (non-iterative) technique. Nominal accuracy for ω is 0.5%. The depth at the coast is always set equal to 1 m, rather than 0, for computational convenience. The stratification values used are generally averaged over 10 or more CTD casts made near the 1000 m isobath. An exponential taper matches the deepest direct observations with deep historical density values.

The numerical approach to finding generalized coastal trapped waves is really only useful for subinertial frequencies. At a frequency at or near f (depending slightly on the offshore boundary condition), a spurious wave mode enters (e.g., Pedlosky, 1979, p. 79) and deflects the physical wave mode dispersion curves in the manner of Allen's (1975) "kissing" modes. At superinertial frequencies, the inertia-gravity wave continuum is discretized by the offshore boundary condition, making the model unrealistic. Thus, free wave dispersion curves are computed only up to $\omega \approx 0.9f$.

b. *Physical aspects of the model*

Several authors (Wang and Mooers, 1976; Clarke, 1977; Huthnance, 1978) have discussed aspects of free generalized coastal trapped waves. Their dis-

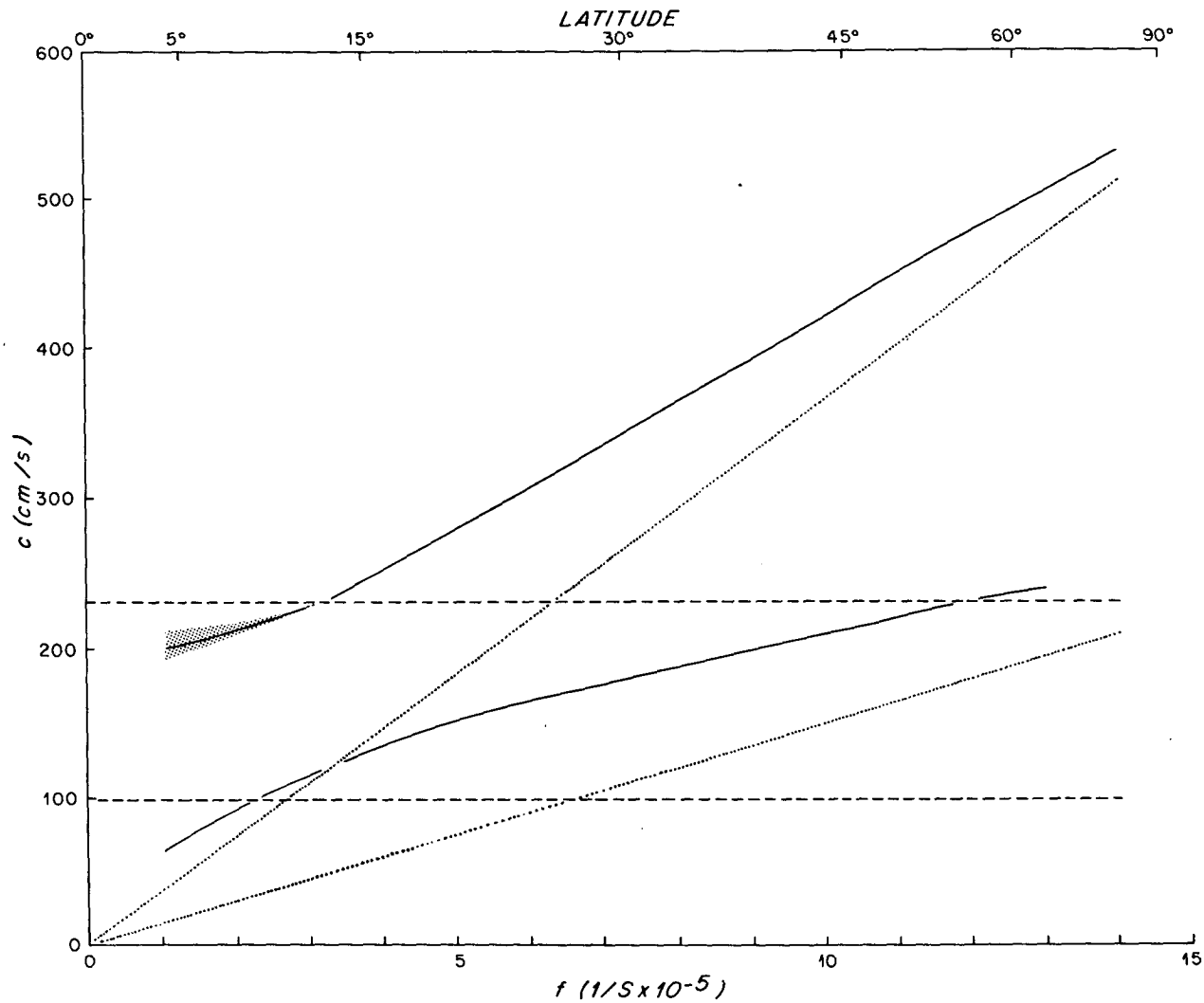

FIG. 2. Long wave phase velocity c versus Coriolis parameter f, calculated using topography and stratification averaged between 12 and 15°S. Latitude corresponding to f is also shown on the horizontal axis. Solid lines: first two hybrid wave modes. Dotted lines: first two barotropic continental shelf wave modes. Dashed lines: first two deep ocean long internal gravity wave modes.

cussions will not be duplicated, but a few aspects which will be useful in interpreting calculations made in reference to the Peru coastal region will be pointed out.

It is illustrative to consider the behavior of the long-wave phase velocity (ω/l) as a function of f, or latitude, holding the topography and stratification fixed. Since the two most important scales of the problem are the internal Rossby radius, which is proportional to f^{-1} and the shelf slope width (Huthnance, 1978), this approach allows a clear demonstration of the phenomenology. The topography and stratification chosen are representative of the region of 12–15°S off Peru. The shelf-slope width Δ is 87 km (depth is held constant at 4000 m farther offshore), and the first mode phase speed c_1 for deep ocean long internal gravity waves is 230 cm s^{-1}. All computations use $l \leqslant 1 \times 10^{-8}$ cm^{-1}, so that $l\Delta \ll 1$. The relative effects of stratification and bottom topography are measured by the stratification parameter [e.g., Huthnance (1978); I have chosen to replace Huthnance's NH with c_1 for the sake of being definite]

$$S = c_1^2(f\Delta)^{-2}, \tag{2.5}$$

which ranges from about 0.04 to 10 in these computations.

Results of the calculations are summarized in Fig. 2. For comparison, dotted lines show the phase speeds of long barotropic continental shelf waves, and dashed lines show c_1 and c_2, the phase speeds of the first two deep ocean (neglecting the shelf and slope) internal Kelvin waves. Solid lines show the first two hybrid wave phase speeds. The shaded area at low

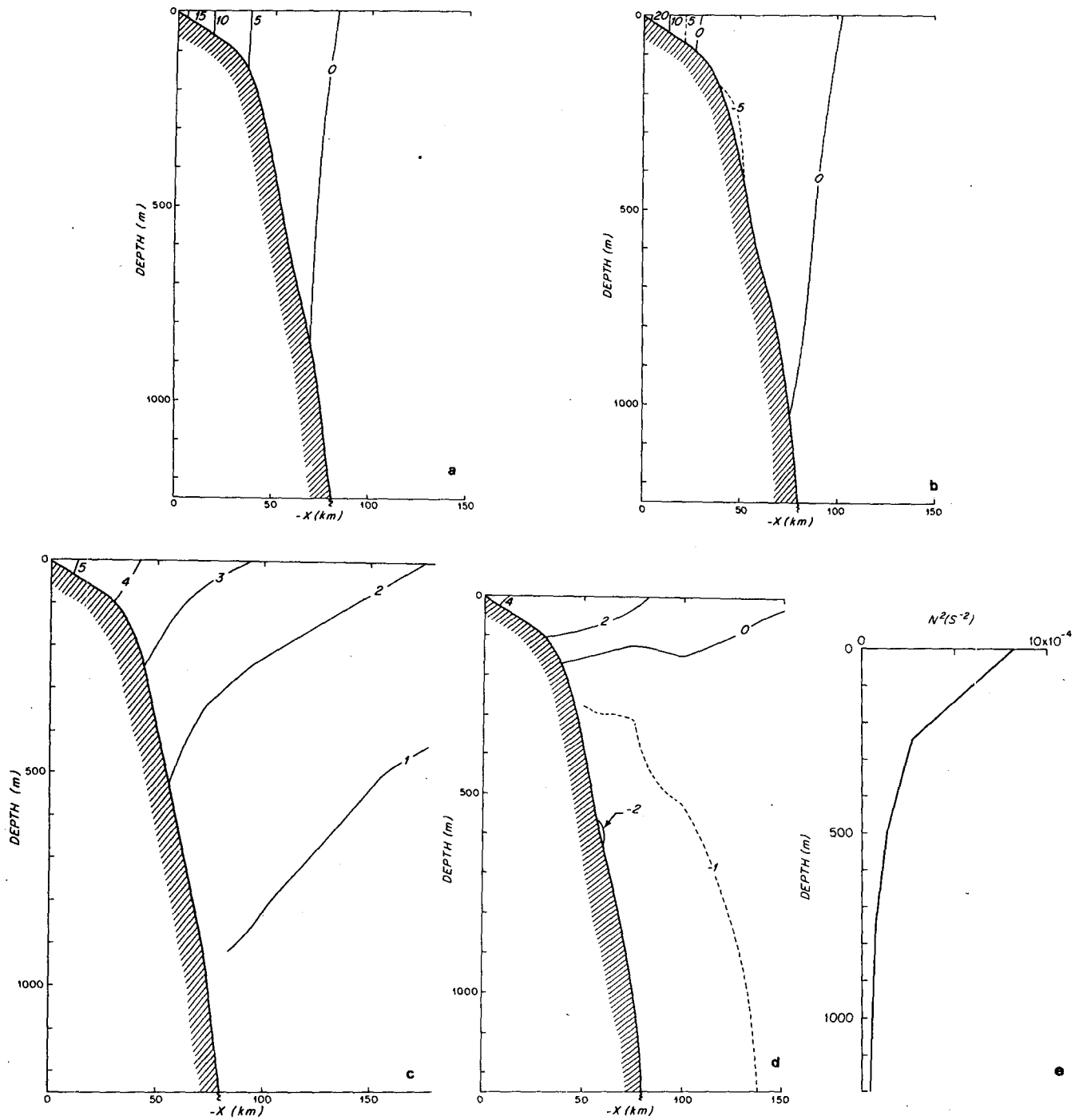

FIG. 3. Pressure structures for long-wave modes, in arbitrary units. Only the upper 1250 m are shown. (a) High-latitude ($f = -14.0 \times 10^{-5}$ s^{-1}) first mode ($c = 531$ cm s^{-1}); (b) high-latitude ($f = 13.1 \times 10^{-5}$ s^{-1}) second mode ($c = 239$ cm s^{-1}); (c) low-latitude ($f = -1.4 \times 10^{-5}$ s^{-1}) first mode ($c = 208$ cm s^{-1}); (d) low-latitude ($f = -1.0 \times 10^{-5}$ s^{-1}) second mode ($c = 65$ cm s^{-1}); (e) profile of N^2 used for the above calculation, averaged in 250 m segments.

f reflects the bounds of computational error, which become particularly large for the first mode at large S. As might be expected (e.g., Allen and Romea, 1980), at high latitudes ($S \approx 0.04$), the generalized phase velocities approach those of barotropic shelf waves, but are somewhat larger (e.g., Clarke, 1977). The high-latitude modal structures (Figs. 3a and 3b) show nearly vertical isopleths over the shelf, consistent with nearly barotropic dynamics. Also, the second mode shows some bottom trapping near the shelf

break, a property commonly associated with topographic waves in a stratified fluid (e.g., Rhines, 1970). The ratio R formed by comparing the spatially integrated wave kinetic and potential energies can also be a useful diagnostic for long waves (Appendix B). For barotropic shelf waves, kinetic energy dominates and R is large. This parameter is 9.1 and 5.1 for the high-latitude $n = 1$ and 2 waves, respectively, suggesting that both modes, and especially the first, have shelf wave-like dynamics. (In the following, "shelf-like" and "Kelvin-like" will be used as abbreviations for "barotropic shelf wave-like" and "internal Kelvin wave-like".)

At low latitudes ($S \approx 4$), the modal behavior changes considerably. The first wave mode (Fig. 3c) can clearly be identified with an internal Kelvin wave: the isopleths slant outward considerably, $R = 2.0$, and at midshelf (30 km from shore, at the surface) the local acceleration term of (2.1b) is 132 times as large as the Coriolis term, approaching pure internal Kelvin wave dynamics where $u \equiv 0$. Note, however, that the phase velocity is less than that of the deep ocean Kelvin wave. The decreased speed is apparently due to the shallower water nearshore, where the local long internal gravity wave speed is considerably decreased: the low-latitude Kelvin wave "feels" a cross-shelf weighted average of the local gravity wave speeds. At extremely low latitudes, the phase speed should again approach that of a Kelvin wave, as the shelf width becomes small relative to the Rossby radius. This effect was demonstrated for barotropic Kelvin waves by Miles (1972), and consideration of a two-layer step shelf model (e.g., Kajiura, 1974) shows the same effect. The decreased Kelvin wave speed was not obtained, for example, by Allen and Romea (1980) because their two-layer model assumed a very shallow upper layer, so that the internal gravity wave speed was always insensitive to the lower layer depth. The second wave mode at low latitude (Fig. 3d) appears more ambiguous. The c-f curve at low latitudes tends to parallel that of the first-mode shelf wave. However, the nearly horizontal isopleths suggest a Kelvin-like structure, and v_t and fu do not tend to balance at mid-shelf: $\omega v(lu)^{-1} = +9.4$. Finally, $R = 2.3$, so that this mode does appear to be more nearly like an internal Kelvin wave.

In summary, the relative magnitudes of the shelf width and of the internal Rossby radius appear to determine the first-mode free wave dynamics. For small S (high latitude in this example), the wave is approximately a barotropic continental shelf wave with its phase speed enhanced by stratification. For large S (low latitude), the behavior is Kelvin-like, but the phase velocity is not well represented by that of a flat-bottom, deep-ocean long internal wave. Thus, even for $S > 1$, the shelf-slope topography is crucial in determining the first-mode phase velocity.

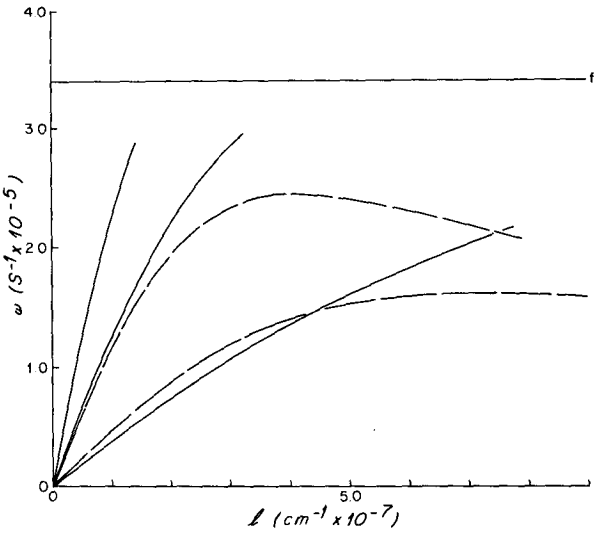

FIG. 4. Dispersion curves for topography, stratification and f averaged between 12 and 15°S. Solid lines: first three hybrid wave modes. Dashed lines: first two barotropic continental shelf wave modes.

The changing character of the first wave mode with latitude is consistent with the results of Allen and Romea (1980), in that the wave mode properties change from Kelvin-like to shelf-like with increasing latitude.

3. Comparison of the wave model and observations

a. Propagation speed

The observations reported by Smith (1978) and RS indicate that between 12 and 15°S the coastal trapped waves are free and propagate nondispersively at about 200 km day^{-1} (230 cm s^{-1}). Thus, the obvious first comparison between theory and observation is the long wave speed in this region. Fig. 4 shows the dispersion curves of the first three wave modes computed for topography, stratification and f averaged between 12 and 15°S. For comparison, the first two barotropic shelf wave dispersion curves are also shown as dashed lines. The first three generalized modes are all nearly nondispersive, with long wave phase speeds of 228, 125, and 37 cm s^{-1}, sequentially. The agreement of the first-mode phase speed with observations is remarkable considering the simplifications of the model, such as neglect of a mean flow. The close phase speed agreement suggests that the first wave mode dominates the propagating variance over this stretch of the Peruvian coast. Also, estimates of first-mode long-wave velocities for other sections of the coast, (Table 4) also tend to be near 230 cm s^{-1}, in agreement with observations reported in RS.

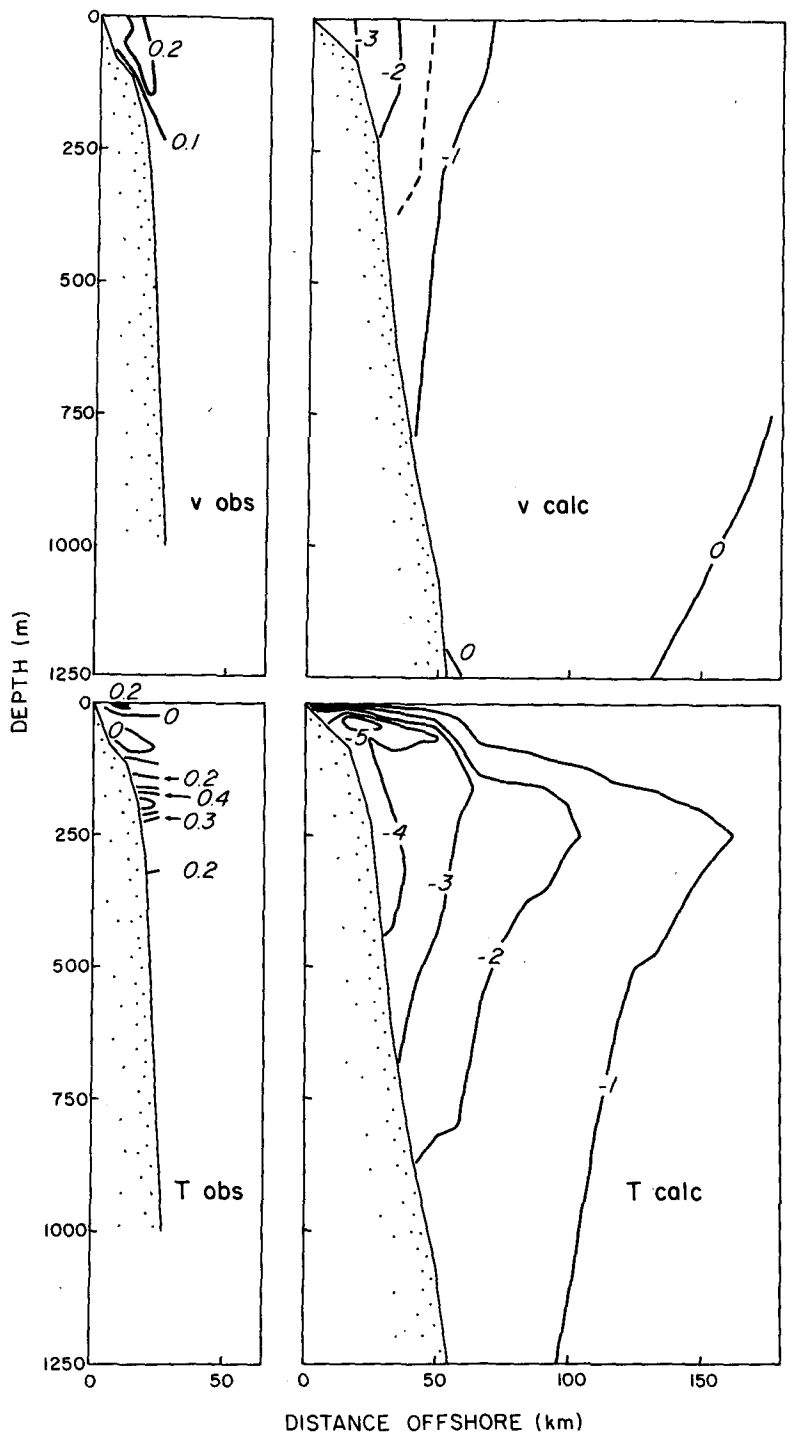

FIG. 5. A comparison of observed and calculated free wave modal structures near 15°S. Only the upper 1250 m are shown. All units are arbitrary. (a) First empirical orthogonal mode of alongshore velocity, representing 54% of the total observed variance along the C-line; (b) alongshore velocity structure associated with the calculated first long free wave mode; (c) second empirical orthogonal mode of temperature fluctuations, representing 22% of the total observed variance along the C-line; (d) temperature fluctuation structure associated with the calculated first long free wave mode.

TABLE 1. Relation of alongshore current to sea level ($v = a\zeta$) at the C-line.

Location	a (s^{-1}) from regression	a (s^{-1}) from model
Mila (59 m)	−2.4	−3.3
Ironwood (63 m)	−2.8	−3.0
Lobivia (183 m)	−2.5	−2.3

b. *Local consistency*

If the coastal trapped waves observed at 15°S are free and mainly represented by the first wave mode, we can compare observations with the structure of the first computed mode. The theoretical mode appears to be dynamically more nearly like an internal Kelvin wave than like a shelf wave ($R = 2.0$), although the topographic scale and the deep ocean Rossby radius are comparable ($S = 0.8$).

At first sight (Fig. 5), the agreement between the observed [empirical orthogonal functions using all C-line records (see BHS)] and the calculated modal structures is not good. The bottom topographies vary slightly because the theoretical modal calculation used bathymetry averaged over 30 km centered on the C-line, but this alone cannot explain the differences. The calculated alongshore velocity mode (Fig. 5b) appears barotropic over the shelf, and $|v|$ decreases monotonically offshore from the coast until a zero crossing occurs well below 500 m depth. The observed wave v structure (Fig. 5a) clearly shows reduced values near the bottom over the shelf, consistent with the presence of bottom friction, an effect neglected in the model. Also, the observed modal structure has its maximum near the shelf break, and decreases toward the coast as well as offshore. This disparity, again, can probably be rationalized in terms of frictional effects. There are, however, two points of agreement. First, the observed v modal structure does not show a zero crossing in the upper 512 m, consistent with the deep node in the calculated mode. Second, away from the region of obvious bottom frictional effects, the observed v structure over the shelf is relatively depth-independent.

Since fluctuations in density near 15°S are well represented by temperature variations (Brink *et al.*, 1979), we can compare the temperature wave empirical mode (Fig. 5c) with the theoretical density mode (Fig. 5d). There are two points of disagreement. First, the observed mode shows substantial structure near the surface, apparently reflecting energetic mixed-layer effects "contaminating" the wave-like empirical mode. Although both the calculated and observed structures show density fluctuation maxima near 20 km from shore, the theoretical maximum is at about 40 m depth, but the observed peak is near 200 m, with a minimum near 80 m. This apparently reflects horizontal variation in the mean stratification, which is considerably weaker over the shelf than farther offshore (roughly 40–60 km from the coast) where the model N^2 was obtained (BHS). Since density fluctuations are strongly dependent on the local stratification [Eq. (2.1e)], this would appear to account for the structural differences.

Some quantitative comparisons are also possible. The observed alongshore velocity component and sea level at San Juan show a good negative correlation suggestive of geostrophy (BHS). This suggests comparison of the observed regression coefficient a between alongshore velocity and corrected (observed plus atmospheric pressure) sea level ζ, where

$$v = a\zeta, \tag{3.1}$$

with the value of a predicted by the model calculations for 15°S. The results are shown in Table 1. Agreement is good near the shelf break (Ironwood) and over the slope (Lobivia), where frictional effects are not expected to strongly affect modal structure. At midshelf (Mila), agreement is poorer, in accord with the qualitative comparison of modal structures.

It is also possible to compare the alongshore momentum balance [Eq. (2.1b)] between observation and theory. First, the relative magnitudes, $|fu|/|v_t|$, $|p_{cy}|/|v_t|$, etc., of observed (absolute values taken as standard deviations computed in the time domain using finite differences for derivatives) terms and predicted (directly from model results) terms are compared in Table 2. The relative values of the coastal alongshore pressure gradient [estimated from sea level at San Martin and San Juan (see fig. 6)] p_{cy} agree crudely in magnitude, and their increasing trend offshore is duplicated by the model. In the calculated model, consistent with a long internal Kelvin wave, the onshore flow is unimportant in the momentum balances. This is at variance with the substantial values of observed fu terms. It appears that some process other than long coastal trapped waves is dominating the onshore flow component. Table 3 shows representative values of correlations involving observationally estimated terms in (2.1b). This provides a measure of how well particular pairs of terms balance. Generally, v_t and p_{cy} are well correlated, v_t and fu are not as well correlated, and fu and p_{cy} (estimated over a 200 km stretch of coast) are uncorrelated (see also BHS). This suggests that the v

TABLE 2. Magnitudes of alongshore momentum equation (2.1b) terms relative to v_t.

	Observed	Model	
	v_t, fu, p_{cy}	v_t, fu, p_{cy}	v_t, fu, local p_y
Mila (59 m)	1, 1.46, 0.98	1, 0.04, 1.46	1, 0.04, 0.96
Ironwood (63 m)	1, 2.47, 1.10	1, 0.03, 1.61	1, 0.03, 0.97
Lobivia (183 m)	1, 1.35, 1.26	1, 0.06, 2.06	1, 0.06, 0.94

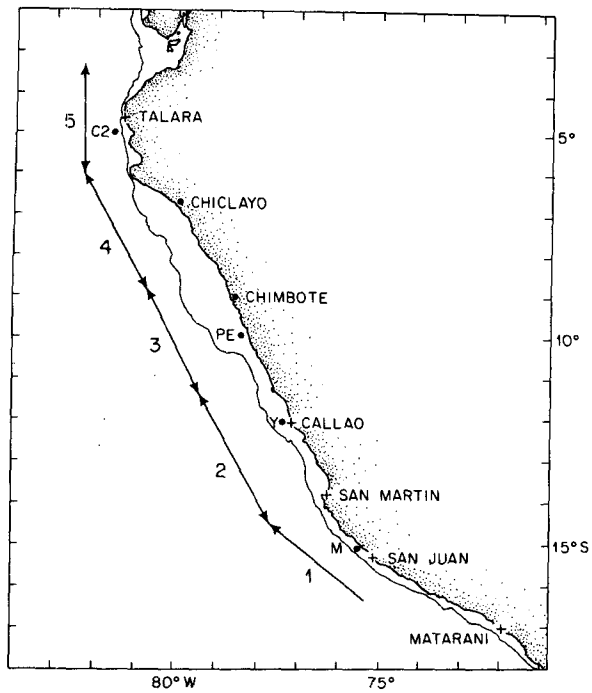

FIG. 6. A map of the Peru coast showing the division into segments for the forced wave calculation. The only depth contour shown is the 200 m isobath. Offshore dots represent current meter moorings: M = Mila, Y = Yucca-Too, Pe = Peyote.

field is dominated by long coastal trapped waves which are adequately finite-differenced over a 200 km separation. The u field, however, seems to be dominated by a process of short (~20 km) alongshore scale, since fu is uncorrelated with the large-scale p_{cy} and because alongshore (u, u) correlation scales are less than 25 km (BHS). The physics which dominates u is undoubtedly reflected to some extent in the v field since the (v_t, fu) correlations are often significant, especially over the shelf. Two processes seem particularly likely to explain the small-scale flow: topographic scattering of long waves or of the mean flow to cause very short scale coastal trapped waves (e.g., Martell and Allen, 1979); and small-scale locally wind-driven motions. The latter alternative has some supporting evidence, since the onshore flow over the shelf is generally significantly correlated with the local alongshore wind stress in a manner consistent with wind-driven upwelling (BHS). If the wind-driven component of u does have small spatial scales, however, it is likely to be ultimately due to local topographic irregularities. This point makes the distinction between the two ways of obtaining small scale u somewhat vague.

c. *The origin of the coastal trapped waves*

If the long-wave approximation ($f \gg \omega$, $l\Delta \ll 1$) for coastal trapped waves applies, it becomes simple, in principle, to predict currents and sea level along the coast, a concept pointed out by Gill and Clarke (1974). In this case, it is possible to expand the total pressure field in terms of the free wave modes

$$p = \sum_{n=0}^{\infty} F_n(x, z)\phi_n(y, t), \tag{3.2}$$

where F_n, c_n is a free wave mode, long wave phase speed pair. If it is somewhat arbitrarily assumed that only the $n = 1$ wave mode (the $n = 0$ mode is the barotropic Kelvin wave) is excited, the disturbances are governed by

$$-\phi_{1y} + c_1^{-1}\phi_{1t} + a_{11}\phi_1 = b_1\tau_0^y, \tag{3.3}$$

where b_n is a wind coupling coefficient, τ_0^y the alongshore component of wind stress, and a_{11} a damping coefficient. Brink (1982) derived a method of computing the bottom frictional contribution to a_{11}. As pointed out by Gill and Clarke (1974), however, other processes, such as topographic scattering and Rossby wave leakage, can also contribute to a_{11}. If the coefficients c_1, a_{11} and b_1 are slowly varying in the alongshore direction, it is possible to solve (3.3) in terms of the characteristic coordinates

$$s = t - \int_y^0 c_1^{-1}dy' \tag{3.4a}$$

and

$$\xi = y. \tag{3.4b}$$

The resulting ordinary differential equation is then integrated to obtain (for $y < 0$)

$$\phi_1(y, t) = \phi_1\left(0, t - \int_y^0 c_1^{-1}d\xi\right)\exp\left(-\int_y^0 a_{11}d\xi\right) + \int_y^0 b_1(\xi)\tau_0^y\left(\xi, t - \int_y^\xi c_1^{-1}d\xi'\right) \times \exp\left(-\int_y^\xi a_{11}d\xi'\right)d\xi, \tag{3.5}$$

where $y = 0$ represents the starting point of the calculation.

In order to carry out the computation (3.5) the Peru coast was first broken into five segments (Fig. 6), each roughly centered on a location where wind measurements were available. Useful input was not available equatorward of section 5. For each seg-

TABLE 3. Observed correlations of terms in the alongshore momentum equation (2.1b) at the C-line.

	v_t, fu	v_t, p_{cy}	fu, p_{cy}
Mila (59 m)	−0.28*	−0.30*	−0.11
Ironwood (63 m)	0.02	−0.44*	−0.19
Lobivia (183 m)	−0.10	−0.22	−0.16

* Correlation significant at the 95% confidence level.

TABLE 4. Properties of the first wave mode in different Peru coastal segments.

Property	Segment 1	2	3	4	5
S	0.7	0.3	0.3	0.9	5.6
R	1.7	2.4	3.0	1.6	1.0
c_1 (cm s^{-1})	236	276	285	227	186
b_1 (cm$^{-1/2}$)	5.5×10^{-3}	6.5×10^{-3}	8.1×10^{-3}	6.8×10^{-3}	4.3×10^{-3}
a_{11} (cm^{-1})	3.3×10^{-9}	3.8×10^{-9}	7.5×10^{-9}	5.6×10^{-9}	1.7×10^{-9}
T_F (days)	15	11	5	9	38
v_{rms} (cm s^{-1})	10	12	17	14*	11
$\Delta\xi$ (km)	209	406	342	275	277

* Interpolated from moorings C-1 and Peyote.

ment, the first long wave free mode was computed, along with c_1, a_{11} and b_1, following Brink (1982), using $C_D \approx 3 \times 10^{-3}$ in the bottom stress law. It should be noted, however, that there is some uncertainty in the values of a_{11} because C_D is not actually known. Table 4 presents some results of these calculations. The wave character varies somewhat from region to region: section 3 has a fairly wide shelf, and the wave mode is relatively shelf-like in character (R = 3.0); section 5 has a relatively narrow shelf, and the wave mode is distinctly Kelvin-like (R = 1.0) and is consequently only weakly affected by bottom friction. One point quickly follows from Table 4: frictional effects are weak enough that $\exp(-\int_y^\xi a_{11} d\xi')$ is always greater than 0.5 for any point north of 15.5°S. That is, signals entering the northern end of segment 5 lose only 50% of their amplitude directly through bottom friction before reaching 15.5°S, a distance of over 1500 km. Thus, the quality of the prediction obtained from (3.5) will be critically dependent on the input information $\phi_1(0, t - \int_y^0 c_1^{-1} d\xi)$. This relatively weak damping also suggests that waves originating at the equator will probably be important at least as far south as San Juan.

As mentioned above, the Peru coastal region was broken up into five segments of varying lengths $\Delta\xi$ (Table 4). For segment 1, the wind record used was from the PSS mooring, located over the inner shelf (BHS). For segment 2, winds recorded by CUEA at the IMARPE building in Callao were used (Enfield *et al.* 1978). For the remaining coastal sections, airport wind records were used. After some experimentation, data from the 5°S midslope C-2 mooring at 86 m were used for the input condition $\phi_1(\xi, s)$ in (3.5). Predicted time series, typically 35 days in length, were calculated for Peyote (10°S) and Mila (15°S) alongshore current, and for Callao (12°S), San Martin (14°S) and San Juan (15.5°S) sea level. All time series had their means removed and represent daily averages. In each case, a prediction was made using as input both the 5°S currents and coastal winds, only the 5°S currents, and only the coastal winds. This allows a clear evaluation of what components of the predicted variance are wind-driven between 5°S and the measurement point, or propagate in from equatorward of 5°S.

Results of the various calculations are compared to their respective observations in Table 5, and the observed and predicted time series for v at 59 m depth at the Mila mooring are shown in Fig. 7. The frequency band of greatest interest is that centered on 0.15 cpd, representing the center of the 5–10 day band where Smith (1978) observed propagation in 1977. Except for the Peyote velocity, predicted standard deviations are the same order of, but slightly smaller than, observed amplitudes. In all cases, the integrated wind driving accounts for no more than 25% of the amplitude of the entire predicted time series. The small size of the wind-driven contribution appears to be due mainly to the relatively weak wind stress *fluctuations* (typically ~0.30 dyn cm^{-2}) along the Peru coast. Predicted and observed amplitudes tend to be well-matched, and wave band coherences are fairly high (especially at San Martin and San Juan), but visual agreement of prediction and observation is not impressive. (Fig. 7, showing the Mila prediction represents the visually *best* case.) Since amplitudes are reasonable, the one-mode assumption is apparently fairly valid and the values of a_{11} and b_1 from theory are probably well estimated. Inspection of Fig. 7 shows that the model predicts some events reasonably well, e.g., around 7–13 April and 1–10 May. During the central part of the record, however, agreement is not very good. This may perhaps be attributable to poor quality (with perhaps anomalously low amplitude) airport wind records, to wave dispersion, or to a general randomization of the wave signal due to scattering by topographic irregularities (e.g., Brink, 1980). Finally, the presence of significant higher wave modes cannot be entirely excluded. It does seem fair to conclude, though, that the first wave mode is dominant and that the sea level and alongshore velocity fluctuations in the region between 12 and 15.5°S are largely governed by first-mode free coastal trapped waves.

TABLE 5. Results of the first-order wave equation integration.

	Location				
	v Peyote (56 m)	ζ Callao	ζ San Martin	v Mila (59 m)	ζ San Juan
Observed standard deviation	6.0 cm s^{-1}	3.5 cm	3.0 cm	9.9 cm s^{-1}	2.7 cm
a. Full calculation					
standard deviation	11.0 cm s^{-1}	2.6 cm	2.4 cm	7.7 cm s^{-1}	2.0 cm
coherence squared and phase					
0.06 cpd	0.34∠ 39° ± 35°	0.40∠ 36° ± 35°	0.33∠ 55° ± 38°	0.09∠ —	0.19∠ 33° ± 53°
0.16 cpd	0.46∠ −48° ± 34°	0.50∠ 30° ± 32°	0.86*∠ 21° ± 8°	0.46∠ −6° ± 34°	0.75*∠ 16° ± 18°
0.27 cpd	0.26∠ −104° ± 45°	0.03∠ —	0.04∠ —	0.13∠ 0° ± 57°	0.77*∠ −65° ± 18°
correlation	0.38	0.21	0.20	0.43*	0.19
maximum lagged**	0.42*/−1 day	0.31/+1 day	0.24/+1 day	—	—
b. No wind input					
standard deviation	10.7 cm s^{-1}	2.4 cm	2.3 cm	7.0 cm s^{-1}	1.8 cm
coherence squared and phase					
0.06 cpd	0.31∠ 43° ± 41°	0.46∠ 34° ± 34°	0.39∠ 52° ± 36°	0.15∠ −14° ± 56°	0.23∠ 29° ± 48°
0.16 cpd	0.52∠ −50° ± 30°	0.44∠ 25° ± 34°	0.84*∠ 17° ± 11°	0.57∠ −10° ± 26°	0.79*∠ 18° ± 17°
0.27 cpd	0.28∠ −110° ± 45°	0.02∠ —	0.07∠ —	0.07∠ —	0.88*∠ −83° ± 8°
correlation	0.34	0.29	0.31	0.50*	0.30
maximum lagged**	0.39/−1 day	0.38/+1 day	0.31/+1 day	—	—
c. Wind input only					
standard deviation	1.1 cm s^{-1}	0.4 cm	0.5 cm	1.7 cm s^{-1}	0.5 cm
coherence squared and phase					
0.06 cpd	0.59∠ 1° ± 26°	0.05∠ —	0.12∠ −168° ± 58°	0.19∠ −169° ± 53°	0.04∠ —
0.16 cpd	0.25∠ 96° ± 45°	0.53∠ 63° ± 30°	0.26∠ 71° ± 45°	0.10∠ 124° ± 62°	0.01∠ —
0.27 cpd	0.53∠ 2° ± 30°	0.22∠ 98° ± 48°	0.24∠ 70° ± 45°	0.13∠ −3° ± 57°	0.72*∠ 46° ± 19°
correlation	0.57*	−0.38	−0.43*	−0.12	−0.32
maximum lagged**	0.60*/+1 day	−0.47*/−1 day	−0.49*/−1 day	—	—

* Coherence squared or correlation significant at 95% confidence. Phase is positive for predicted leading observed. Error on phase is at 95% confidence. Phases are not given for coherence squared less than 0.1.

** Maximum lagged correlation (if not at zero lag), and lag time in days. Lag is positive for predicted time series leading observed.

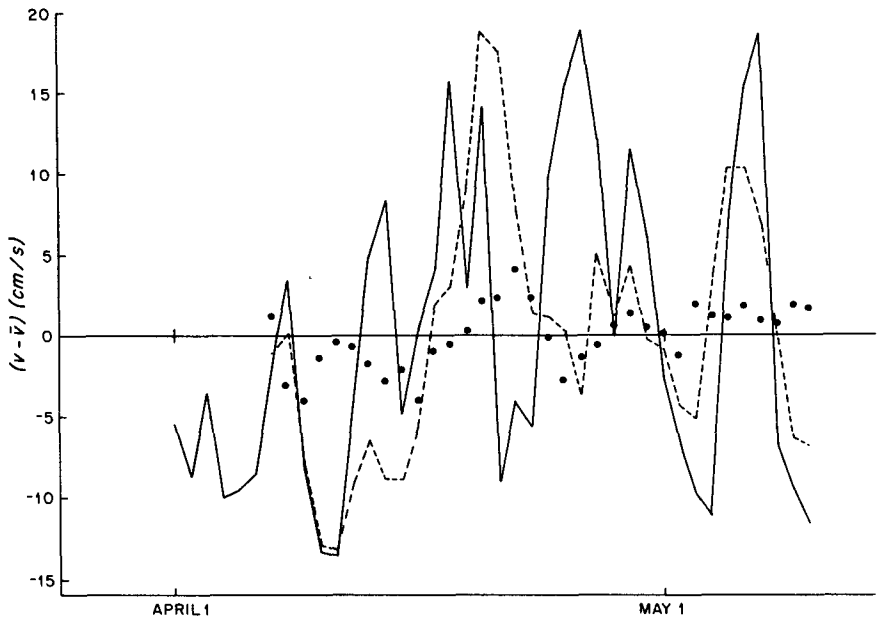

FIG. 7. Observed versus predicted current fluctuations at 59 m depth at the midshelf Mila mooring near 15°S. Positive values correspond to flow toward the northwest. Solid line: observed time series. Dashed line: total predicted time series. Dotted line: wind-driven contribution to the predicted time series.

Finally, some comment is called for on the limited frequency range of agreement between the predicted and observed time series (Table 5). The validity of the wave theory is tightly constrained by the assumptions that wave frequency be much greater than the inverse frictional decay time (Brink, 1982), and that the low-frequency ($f^2 \gg \omega^2$) approximation be everywhere valid. In fact, the parameters in Table 4 suggest that there is no frequency band where, along the entire coast, these two constraints are both strictly satisfied. It may be that the forced, frictional, long-wave theory is sufficiently robust that local violations of model assumptions are not critical.

d. Coastal trapped waves in other CUEA regions

The CUEA program made intensive physical observations off both Oregon (Kundu *et al.*, 1975) and Northwest Africa (Mittelstaedt *et al.*, 1975), as well as off Peru. In the two former regions, fluctuations in alongshore velocity over the shelf were generally closely related to the local alongshore wind stress. Off Oregon, several studies have also reported the presence of coastal trapped waves with phase speeds of 400–500 cm s^{-1} (e.g., Mooers and Smith, 1968; Kundu and Allen, 1976), although Hickey (1982) has questioned the free wave interpretation. Off Northwest Africa, current measurements have not revealed free coastal trapped waves, partly because currents are so clearly related to the local wind, and partly because of a lack of any observational resolution in the alongshore direction. The wave model of Section 2 can be used to attempt to rationalize the differing wave climates.

The Northwest African case (summarized in Table 6) is perhaps the simplest. Due to the large near-bottom speed (v_{rms}) over the shelf, frictional effects are so strong that the modified first-order wave equa-

TABLE 6. Comparison of first mode wave properties among the three CUEA regions.

	Oregon (Jul–Aug 1973)	Northwest Africa (Feb–Apr 1974)	Peru (Mar–May 1977)
Central latitude	45.25°N	21.5°N	14.5°S
S	0.02	0.20	0.83
R	10.0	4.4	1.7
c_p (cm s^{-1})	490	275	236
b_1 ($cm^{-1/2}$)	0.72×10^{-2}	1.09×10^{-2}	0.55×10^{-2}
a_{11} (cm^{-1})	1.8×10^{-9}	13×10^{-9}	3.3×10^{-9}
T_F (days)	13	3	15
v_{rms} (cm s^{-1})	10	19	10
Standard deviaton of τ^y (dyn cm^{-2})	0.53	0.74	0.35
Predicted locally wind-driven midshelf v (cm s^{-1})	3	10	1
Observed standard deviation of midshelf v (cm s^{-1})	11	12	9

tion (3.3) is no longer strictly valid. Thus, free, nearly inviscid coastal trapped waves are unlikely to exist. As an order of magnitude check, the locally wind-driven velocity over the shelf can be estimated by balancing the local time change term with the wind stress in (3.3). This yields

$$v \approx q\omega^{-1}c_1 b_1 \tau^y, \tag{3.6}$$

where q is a scaling factor derived from the free wave modal structure. For a typical period of 10 days, (3.6) yields an estimated midshelf, mid-depth locally wind-driven standard deviation of alongshore velocity of $\sim$10 cm s^{-1} (Table 6). This is comparable with the observed value of 12 cm s^{-1}, suggesting that most of the variance over the shelf should indeed be locally wind-driven. The apparent reasons for this are the large coupling coefficient b_n, strong bottom friction, and the substantial variance of the local wind stress. The above reasons are somewhat interdependent because strong winds and efficient coupling naturally lead to large induced speeds, hence strong bottom friction.

The Peru case has been discussed to some extent above. The weak winds and coupling lead to an estimated [by (3.6)] wind-driven midshelf scale speed of only 1 cm s^{-1} at 15°S, compared to the observed total of 9 cm s^{-1} (Table 6). This order-of-magnitude estimate, combined with the relatively long spin-down time, reaffirms that free waves should play an important role in this region.

The Oregon 1973 summertime example represents an intermediate case with respect to wind driving. The first long free wave is nearly barotropic: S = 0.02 and R = 10.0. The wind coupling and the frictional effects are both intermediate to the Peru and Northwest African cases, and the estimated (from 3.6) midshelf alongshore velocities are only about one-quarter of the total observed (Table 6). This appears somewhat inconsistent with observations, which indicate that about 54% of the midshelf alongshore velocity fluctuation amplitude is associated with the local alongshore wind stress (Kundu and Allen, 1976), i.e., that the standard deviation of locally wind driven velocity should be about 6 cm s^{-1}, as opposed to the 3 cm s^{-1} from (3.6). One possible explanation for the low estimate of wind-driven currents by (3.6) is the phase speed resonance suggested by Kundu *et al.* (1975). The local winds do appear to migrate northward in some frequency bands (Huyer *et al.*, 1975) at a speed comparable to that of the first mode free wave. This could lead to an enhancement of observed wind-driven currents, and would also appear to be a free coastal trapped wave. This explanation requires, however, that the phase speeds of winds and coastal trapped waves match over at least 1300 km south of 45°N. This appears to be too large a distance to be credible.

Since Oregon represents a case where free coastal trapped waves may be expected, their calculated properties will be briefly discussed. Fig. 8a shows the computed first-mode, long-wave, alongshore velocity structure. The isotachs are nearly vertical over the shelf and slope, consistent with the barotropic shelf wave behavior expected for a relatively wide shelf (S = 0.02). Also, the long-wave phase velocity (Table 6) is only 11% greater than that predicted by a purely barotropic model. The computed dispersion curve (Fig. 8b) shows that stratification is still quite important at shorter wavelengths. The barotropic dispersion curve (dotted line) turns down for larger l, but the generalized wave goes to a higher frequency and levels off to within computational error. Thus, the alongshore group velocity is zero for a fairly broad range of alongshore wavelengths. As a check on how rapidly the barotropic limit is reached, the calculation was repeated using the actual stratification divided everywhere by a factor of 10 (dashed line). Even for this very weak stability, the barotropic curve is not matched exactly. It appears that, for the Oregon shelf, a purely barotropic model is reasonable only in the long-wave limit, and that stratification must be included if general wavelengths are considered. This, in turn, indicates that some quantitative results of dispersive barotropic shelf wave theory applied to the Oregon coast (e.g., Cutchin and Smith, 1973; Brink, 1980; Hsieh and Mysak, 1981) will be invalid, although some qualitative predictions may still obtain, a conclusion also drawn by Wang and Mooers (1976).

4. Conclusions

To a first approximation, it seems that the observed waves off Peru can be treated as free, first-mode, hybrid coastal trapped waves. The comparison between the observed and theoretical wave properties, however, yields mixed results, with phase speeds and sea level–alongshore velocity transfer functions showing the best agreement. The poorest performance of the model was probably on the prediction of the overall modal (x, z) structures. This difficulty appears to be related to the neglect of bottom friction at the lowest order and of horizontal variations in static stability. Luther and Bane (1980) have recently formed an improved model which takes the latter problem into account. The results of the forced long-wave model show fair agreement with observations, given the frequency constraints on the model. The rough agreement of observed and predicted amplitudes lends credibility to the values of the wind coupling and bottom drag coefficients derived in Brink (1982).

It appears that the region off the coast of Peru is a remarkably good locale for observing free coastal trapped waves. The factors which appear to account

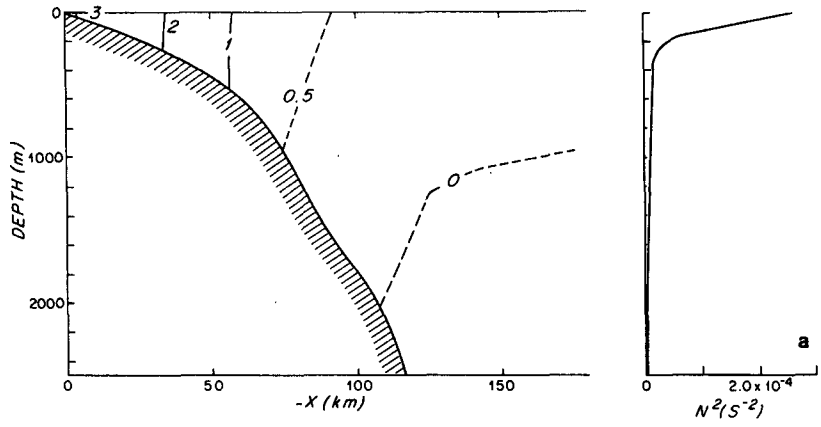

FIG. 8a. Free-wave calculations for an Oregon example, using summertime 1973 stratification. Long-wave phase speed is 490 cm s^{-1}. Alongshore velocity structure associated with the first long free wave mode. Units are arbitrary. Also shown is the N^2 profile used for the calculation, averaged in 150 m segments.

for this are the relatively weak fluctuations in alongshore wind stress, and the relatively weak damping associated with waves where the effect of stratification is dynamically important [$S \geq 1$; see (2.5)]. In regions, such as Northwest Africa, where bottom frictional effects are of lowest order importance, the coastal trapped wave theory employed here appears less useful. Finally, the Oregon example points out the need to consider the effects of stratification in the application of theories which involve dispersive effects in coastal trapped waves.

It is natural to make comparisons with two-layer models of hybrid coastal trapped waves. These models have the considerable advantage of analytical simplicity, and the resulting virtue of clear results. Two specific predictions of these models bear inspection. First, Allen (1975), for example, found that the dispersion (i.e., ω vs l) curves of Kelvin and shelf-like wave modes "kissed", and exchanged dynamical properties. Wang and Mooers (1976) duplicated this behaviour in a continuously stratified model, but only by using an exaggerated geometry with a sufficiently high coastal wall for a flat-bottom type Kelvin wave to exist near the "coast". Models with a more realistic shelf-slope structure given by Wang and Mooers (1976), by Huthnance (1978), and the above do not appear to produce "kissing modes" at all. Rather, each dispersion curve appears to represent a distinct mode which retains its fundamental dynamics. Second, Allen and Romea (1980) found, with a two-layer model, that plots of long-wave phase speed c vs f also tend to show "kissing", with the constant c low-latitude Kelvin mode turning into a high-latitude nearly barotropic shelf mode. The results presented here (Fig. 2) agree in terms of the changing nature of the first mode wave, and seem to show some "kissing". Although the first-mode low-latitude long wave is Kelvin-like, its phase speed still depends upon the presence of bottom topography. It seems that the results of two-layer models can give us considerable insight on the qualitative behavior of coastal trapped waves in a stratified ocean, but that results should be checked against a more realistic model before firm conclusions are drawn.

Finally, it appears that the long coastal trapped wave formalism is indeed a useful tool for the study of motions over the continental shelf. Application of the theory, however, requires considerable attention to the effects of dissipation and of the combination of stratification and bottom topography. In this context, further study is needed for the important parameter ranges which are 1) neither quasi-steady nor nearly inviscid, and 2) where short alongshore scales are allowed.

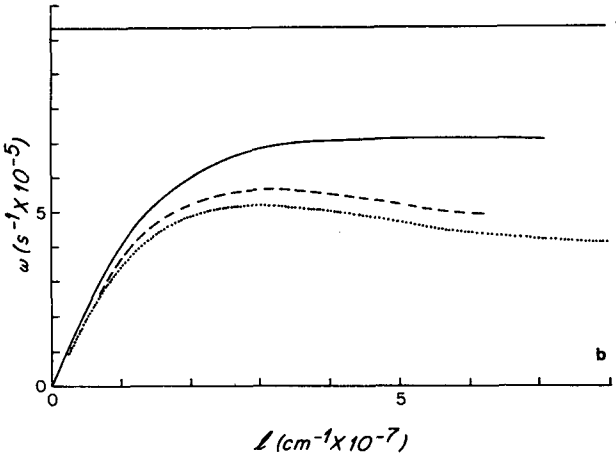

FIG. 8b. As in Fig. 8a except for first-mode dispersion curves as a function of stratification. Solid line: observed stratification. Dashed line: observed stratification decreased everywhere by a factor of 10. Dotted line: barotropic case ($N^2 = 0$).

Acknowledgments. The author benefited considerably from discussions with Dr. J. S. Allen and R. D. Romea. Also, Drs. D. B. Enfield, D. Halpern, A. Huyer and R. L. Smith generously made data available to me. Funding for this work was provided by the Coastal Upwelling Ecosystems Analysis (CUEA) program of the International Decade of Ocean Exploration (IDOE) office of the National Science Foundation (NSF), through Grants OCE 78-03380 and OCE-80-24116. Some support at the writing stage was also provided by the Coastal Research Center, Woods Hole Oceanographic Institution.

APPENDIX A

Test of Offshore Boundary Conditions

A simple analytical model which allows both shelf-like and internal Kelvin-like waves will be used to test the effect of various offshore boundary conditions on a numerical model. The physical model employed is a simplification of one considered by Kajiura (1974). The step-shelf geometry for the analytical example is shown in Fig. 9. We consider a two-layer ocean rotating about its vertical axis at a constant effective rate of $f/2$. The model neglects nonlinearity, viscous effects, and the divergence due to free surface deflections. Only long free coastal trapped waves are considered, i.e., 1) the wave frequency ω is assumed to be much less than f, and 2) the alongshore wavelength $2\pi l^{-1}$ is assumed to be large relative to the shelf width Δ and to the internal Rossby radius λ. Subject to these assumptions, the depth-integrated equations of motion over the shelf ($x > -\Delta$) are

$$-fV = -gh\zeta_x, \tag{A1.1a}$$

$$V_t + fU = -gh\zeta_y, \tag{A1.1b}$$

$$U_x + V_y = 0. \tag{A1.1c}$$

Away from the shelf, we assume that the lower layer is very deep relative to the upper layer, so that motions below the interface can be neglected. The depth-integrated upper layer equations of motion for $x < -\Delta$ now become

$$-fV = -gH_1\zeta_x, \tag{A1.1d}$$

$$V_t + fU = -gH_1\zeta_y, \tag{A1.1e}$$

$$U_x + V_y = -\epsilon^{-1}\zeta_t, \tag{A1.1f}$$

where U and V are the depth-integrated onshore and alongshore velocity components, respectively, ζ is the free surface deflection (positive upwards), g the acceleration due to gravity, h and H_1 the upper layer depths over the shelf and in the deep ocean, respectively, and ϵ the fractional density difference across the interface.

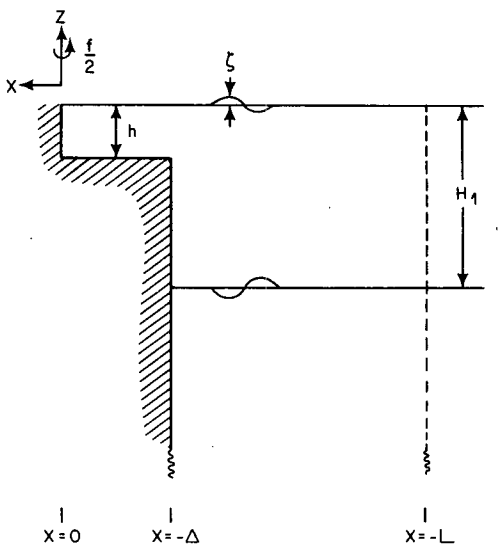

FIG. 9. Schematic of the model geometry used to test for offshore ($x = L$) boundary conditions.

We now seek solutions of the form

$$\{U, V, \zeta\} = [\hat{U}(x), \hat{V}(x), \hat{\zeta}(x)] \exp[il(y + ct)], \tag{A1.2}$$

where c is the alongshore phase velocity. The problem is solved subject to

$$\hat{U} = 0 \quad \text{at} \quad x = 0, \tag{A1.3a}$$

$$\hat{U}, \hat{\zeta} \text{ are continuous} \quad \text{at} \quad x = -\Delta, \tag{A1.3b,c}$$

and a variety of conditions at $x = -L$, the offshore boundary. We seek the formulation which best approximates the physical coastal trapping condition:

$$\zeta \to 0 \quad \text{as} \quad x \to \infty. \tag{A1.4a}$$

The particular offshore conditions to be tested are

$$\hat{\zeta} = 0 \quad \text{at} \quad x = -L, \tag{A1.4b}$$

$$\hat{\zeta}_x = 0 \quad \text{at} \quad x = -L, \tag{A1.4c}$$

$$\hat{U} = 0 \quad \text{at} \quad x = -L, \tag{A1.4d}$$

$$\hat{U}_x = 0 \quad \text{at} \quad x = -L, \tag{A1.4e}$$

$$\hat{\zeta}_x + cfc_0^{-2}\hat{\zeta} = 0 \quad \text{at} \quad x = -L, \tag{A1.4f}$$

where c_0 is the long internal gravity wave speed, $(\epsilon g H_1)^{1/2}$. The first test condition is that used by Wang and Mooers (1976), and the fifth test condition, that internal Kelvin wave physics obtain, is analogous to the condition used by Huthnance (1978).

It is now straightforward to solve (A1.1)–(A1.4) and obtain an equation for the long-wave phase velocities for each of the boundary conditions. The equation describing the long-wave phase velocities

TABLE A1. Coefficients of Eq. (A1.5) for different offshore boundary conditions.*

Boundary conditions		a_1	a_2	a_3
physical	(A1.4a)	$-(c_0 + f\Delta)$	$f\Delta c_0 Q$	0
$\hat{\zeta} = 0$	(A1.4b)	$-(c_0 T + f\Delta)$	$f\Delta c_0 Q$	0
$\hat{\zeta}_x = 0$	(A1.4c)	$-(c_0 T^{-1} + f\Delta)$	$f\Delta c_0 Q T^{-1}$	0
$\hat{U} = 0$	(A1.4d)	$-f\Delta$	$-c_0(c_0 + hf\Delta H_1^{-1} T^{-1})$	$f\Delta c_0^2 Q$
$\hat{U}_x = 0$	(A1.4e)	$-f\Delta$	$-c_0(c_0 + hf\Delta H_1^{-1} T)$	$f\Delta c_0^2 Q$
$\hat{\zeta}_x + cfc_0^{-2}\hat{\zeta} = 0$	(A1.4f)	$-f\Delta$	$-c_0(c_0 + hf\Delta H_1^{-1} T)$	$f\Delta c_0^2 Q$

* $\begin{cases} T = \tanh[\lambda^{-1}(L - \Delta)], \\ Q = (H_1 - h)H_1^{-1}. \end{cases}$

is

$$0 = c^3 + a_1 c^2 + a_2 c + a_3 , \qquad \text{(A1.5)}$$

where the coefficients a_1, a_2 and a_3 are given in Table A1 for each of the choices of boundary conditions. Conditions (A1.4d)–(A1.4f) all allow three values of c: an internal Kelvin wave with $c < 0$ may exist near the $x = -L$ boundary. For all of the cases, the solutions approach the physical ($\hat{\zeta} \to 0$ as $x \to \infty$) values as

$$T = \tanh[\lambda^{-1}(L - \Delta)] \qquad \text{(A1.6a)}$$

($\lambda = c_0 f^{-1}$) approaches unity. That is, if the width of the deep ocean region is large relative to the Rossby radius, the phase velocities become insensitive to the particular boundary condition chosen. Also, for long waves, conditions (A1.4e) and (A1.4f) are equivalent.

Particular problems arise, however, at low latitudes ($f \to 0$), where the Rossby radius can become quite large. In this case, we can expand (A1.6a), for fixed L and Δ, to

$$T \approx fc_0^{-1}(L - \Delta),$$

and investigate the values of c for $f \to 0$. This is not a completely realistic limit to take, since the long-wave assumption becomes overly restrictive for small f, but the results are still interesting. At low latitudes, the physical solution consists of a Kelvin wave, $c = c_0$, independent of f, and a shelf wave with c proportional to f. Not all of the boundary conditions (A1.4b)–(A1.4f) have this behavior, however, as indicated by Table A2. In fact, only the last two boundary conditions, $\hat{U}_x = 0$ and the Kelvin wave-like condition, have the proper asymptotic behavior.

TABLE A2. Long-wave phase velocities for $f \to 0$.

Boundary condition		c
physical	(A1.4a)	$0, c_0$
$\hat{\zeta} = 0$	(A1.4b)	0, 0
$\hat{\zeta}_x = 0$	(A1.4c)	$0, \infty$
$\hat{U} = 0$	(A1.4d)	$0, \pm c_0\, h\Delta\, H_1^{-1}(L - \Delta)^{-1}$
$\hat{U}_x = 0$	(A1.4e)	$0, \pm c_0$
$\hat{\zeta}_x + cfc_0^{-2}\hat{\zeta} = 0$	(A1.4f)	$0, \pm c_0$

APPENDIX B

The Energy Diagnostic

In the text, it was asserted that the ratio of integrated wave kinetic to potential energies is a useful diagnostic for evaluating the Kelvin wave-like or shelf wave-like nature of a free wave. The following represents a demonstration of this assertion.

First, consider a barotropic case, where the depth-integrated long-wave equations of motion are

$$fV = gh\zeta_x , \qquad \text{(B2.1a)}$$

$$V_t + fU = -gh\zeta_y , \qquad \text{(B2.1b)}$$

$$0 = \zeta_t + U_x + V_y , \qquad \text{(B2.1c)}$$

where ζ is the free-surface height, and U and V are the depth-integrated components of horizontal velocity. The energy equation then becomes

$$(\tfrac{1}{2}h^{-1}V^2 + \tfrac{1}{2}g\zeta^2)_t = -g[(U\zeta)_x + (V\zeta)_y]. \qquad \text{(B2.2)}$$

Integrating this form with respect to x, and using the conditions $U = 0$ at $x = 0$ and U, $\zeta \to 0$ as $x \to \infty$ yields

$$\int_0^\infty (\tfrac{1}{2}h^{-1}V^2 + \tfrac{1}{2}g\zeta^2)_t dx = -\int_0^\infty (Vg\zeta)_y dx. \qquad \text{(B2.3)}$$

This simply states that the time rate of change of integrated kinetic ($\frac{1}{2}h^{-1}V^2$) plus potential ($\frac{1}{2}g\zeta^2$) energy is balanced by the alongshore divergence of integrated energy flux. The potential energy is small relative to kinetic energy for shelf waves by the ratio $f^2\Delta^2 g^{-1}h^{-1}$. Thus, in the rigid lid limit, where the barotropic Rossby radius of deformation is much greater than the shelf width, the potential energy is negligible and

$$R = \frac{\text{kinetic energy}}{\text{potential energy}}$$

approaches infinity.

In the baroclinic case, the long-wave limit of Eqs. (2.1) apply, and the energy equation becomes

$$(\tfrac{1}{2}\rho_0 v^2 + \tfrac{1}{2}g^2 N^{-2}\rho_0^{-1}\rho^2)_t = -[(up)_x + (vp)_y + (wp)_z]. \qquad \text{(B2.4)}$$

This is integrated over all z and x, to obtain, with the use of (2.2)

$$\int_0^\infty \int_{-h}^0 (\tfrac{1}{2}\rho_0 v^2 + \tfrac{1}{2}g^2N^{-2}\rho_0^{-1}\rho^2)_t dz dx + \int_0^\infty (\tfrac{1}{2}g^{-1}\rho_0^{-1}p^2)_t dx\Big|_{z=0} = -\int_0^\infty \int_{-h}^0 (vp)_y dz dx. \quad \text{(B2.5)}$$

The three terms on the left hand side represent kinetic energy, potential energy due to changes in the density field, and potential energy associated with free surface displacements. Written in terms of pressure only, the integrated kinetic energy becomes

$$K = -\tfrac{1}{2}\rho_0^{-1}f^{-2}\left[\int_{-h}^0 pp_x dz\Big|_{x=0} + \int_0^\infty h_x pp_x dx\Big|_{z=-h} + \int_0^\infty \int_{-h}^0 pp_{xx} dz dx\right], \quad \text{(B2.6a)}$$

and the total integrated potential energy becomes

$$P = -\tfrac{1}{2}\rho_0^{-1}\left[\int_0^\infty p\frac{p_z}{N^2}dx\Big|_{z=-h} + \int_0^\infty \int_{-h}^0 p\left(\frac{p_z}{N^2}\right)_z dz dx\right]. \quad \text{(B2.6b)}$$

We now consider the case of a flat bottom, where only Kelvin waves can occur. In this case, the second term in (B2.6a) and the first term in (B2.6b) vanish identically. The pressure for a Kelvin wave can be written as

$$p = F_n(z)\exp(-xf/c_n)\phi_n(y + c_n t), \quad \text{(B2.7)}$$

where F_n and c_n satisfy the eigenvalue problem

$$F_n + c_n^2\left(\frac{F_{nz}}{N^2}\right)_z = 0, \quad \text{(B2.8a)}$$

$$F_{nz} + N^2 g^{-1}F_n = 0, \quad \text{at} \quad z = 0, \quad \text{(B2.8b)}$$

$$F_{nz} = 0, \quad \text{at} \quad z = -h. \quad \text{(B2.8c)}$$

Substitution of (B2.7) into the expressions for K and P, along with the use of (2.2d) yields

$$K = P = \tfrac{1}{4}(f\rho_0 c_n)^{-1}\phi_n^2 \int_{-h}^0 F_n^2 dz.$$

Thus, the expected result of equipartition of potential and kinetic energy ($R = 1$) has been obtained.

In summary, for the barotropic shelf-wave case R is large or infinite (depending on the surface boundary condition), and for the Kelvin wave limit, $R = 1$. It therefore seems reasonable to use the ratio R as a diagnostic of the character of a generalized long free coastal trapped wave. Since short shelf-like waves become bottom trapped in the presence of stratification (Wang and Mooers, 1976), R will also presumably approach unity in this limit. Thus for short waves, R may not be a very discriminating parameter.

REFERENCES

Allen, J. S., 1975: Coastal trapped waves in a stratified ocean. *J. Phys. Oceanogr.*, **5,** 300–325.

——, and R. D. Romea, 1980: On coastal trapped waves at low latitudes in a stratified ocean. *J. Fluid Mech.*, **98,** 555–585.

Brink, K. H., 1980: Propagation of barotropic continental shelf waves over irregular bottom topography. *J. Phys. Oceanogr.*, **10,** 765–778.

——, 1982: The effect of bottom friction on low-frequency coastal trapped waves. *J. Phys. Oceanogr.*, **12,** 127–133.

——, W. E. Gilbert and A. Huyer, 1979: Temperature sections along the C-line over the shelf off Cabo Nazca, Peru, from moored current meters, 18 March–10 May 1977, and CTD observations, 5 March–15 May 1977. CUEA Tech. Rep. 49, School of Oceanography, Oregon State University, 78 pp.

——, D. Halpern and R. L. Smith, 1980: Circulation in the Peruvian upwelling system near 15°S. *J. Geophys. Res.*, **85,** 4036–4048.

Clarke, A. J., 1977: Observational and numerical evidence for wind-forced coastal trapped long waves. *J. Phys. Oceanogr.*, **7,** 231–247.

Cutchin, D. L., and R. L. Smith, 1973: Continental shelf waves: low-frequency variations in sea level and currents over the Oregon continental shelf. *J. Phys. Oceanogr.*, **3,** 73–82.

Enfield, D. B., R. L. Smith and A. Huyer, 1978: A compilation of observations from moored current meters. Vol. XII. Wind, currents and temperature over the continental shelf and slope off Peru during JOINT II. March 1976–May 1977. CUEA Data Rep. 70, School of Oceanography, Oregon State University, 343 pp.

Gill, A. E., and A. J. Clarke, 1974: Wind-induced upwelling, coastal currents and sea level changes. *Deep-Sea Res.*, **21,** 325–345.

Hickey, B. M., 1982: Temporal and spatial variability of the California Undercurrent off Washington during summer 1972. Submitted to *J. Mar. Res.*

Hsieh, W. W., and L. A. Mysak, 1981: Resonant interactions between shelf waves, with applications to the Oregon shelf. *J. Phys. Oceanogr.*, **10,** 1729–1741.

Huthnance, J. M., 1978: On coastal trapped waves: Analysis and numerical calculation by inverse iteration. *J. Phys. Oceanogr.*, **8,** 74–92.

Huyer, A., B. M. Hickey, J. D. Smith, R. L. Smith and R. D. Pillsbury, 1975: Alongshore coherence at low frequencies in currents observed over the continental shelf off Oregon and Washington. *J. Geophys. Res.*, **80,** 3495–3505.

Kajiura, K., 1974: Effect of stratification on long period trapped waves on the shelf. *J. Oceanogr. Soc. Japan.*, **30,** 272–281.

Kundu, P. K., and J. S. Allen, 1976: Some three-dimensional characteristics of low-frequency current fluctuations near the Oregon coast. *J. Phys. Oceanogr.*, **6,** 181–199.

——, J. S. Allen and R. L. Smith, 1975: Modal decomposition of the velocity field near the Oregon coast. *J. Phys. Oceanogr.*, **5,** 683–704.

Luther, M. E., and J. M. Bane, Jr., 1980: Coastal-trapped and frontal-trapped waves in a continuously stratified western boundary current. Tech. Rep. CMS-80-1, University of North Carolina at Chapel Hill, 77 pp.

Martell, C. M., and J. S. Allen, 1979: The generation of continental shelf waves by alongshore variations in bottom topography. *J. Phys. Oceanogr.*, **9**, 696–711.

Miles, J. W., 1972: Kelvin waves on oceanic boundaries. *J. Fluid Mech.*, **55**, 113–127.

Mittelstaedt, E., R. D. Pillsbury and R. L. Smith, 1975: Flow patterns in the northwest African upwelling area. *Dtsch. Hydrogr. Z.*, **28**, 145–167.

Mooers, C. N. K., and R. L. Smith, 1968: Continental shelf waves off Oregon. *J. Geophys. Res.*, **73**, 549–557.

Pedlosky, J., 1979: *Geophysical Fluid Dynamics*. Springer-Verlag, 624 pp.

Rhines, P., 1970: Edge-, bottom-, and Rossby waves in a rotating stratified fluid. *Geophys. Fluid Dyn.*, **1**, 273–302.

Romea, R. D., and R. L. Smith, 1982: Further evidence for coastal trapped waves along the Pacific Coast of South America. Submitted to *J. Phys. Oceanogr.*

Smith, R. L., 1978: Poleward propagating perturbations in currents and sea level along the Peru coast. *J. Geophys. Res.*, **83**, 6083–6092.

Wang, D.-P., and C. N. K. Mooers, 1976: Coastal trapped waves in a continuously stratified ocean. *J. Phys. Oceanogr.*, **6**, 853–863.